INSTITUT CARNOT Ifremer-EDROME	Compte-rendu de fin de projet	référence 06/11/2013 Nbre de pages: 29

Institut CARNOT Ifremer-EDROME

Caracterisation of micro-seismicity in the Western Sea of Marmara: implications for seismic monitoring strategies

Caractérisation de la micro-sismicité dans la partie occidentale de la faille Nord-Anatolienne en Mer de Marmara : implications en termes de stratégie de surveillance de l'activité sismique

Abondement Carnot 2011

IDENTIFICATION

Acronyme du projet	Micro-sismicité en Mer de Marmara
Titre du projet	Caractérisation de la micro-sismicité sous-marine dans la partie occidentale de la faille nord-anatolienne en Mer de Marmara : implications en termes de stratégie de surveillance de l'activité sismique
Nom de l'Institut Carnot	Ifremer Edrome
Période du projet (date de début – date de fin)	02/04/2012 – 30/09/2013
Site web du projet le cas échéant	

Rédacteur de ce rapport	
Civilité, prénom, nom	Estelle CROS - Louis Géli
Téléphone	0298224227 / 0298498757
Adresse électronique	geli@ifremer.fr - estellcros@gmail.com
Date de rédaction	Octobre 2013

Budget total du projet	**76639 Euros**
Part pris sur l'abondement 2011	L'abondement Carnot a esentillement servi à co-financer le post-doc d'Estelle Cros. L'autre demi-financement a été assuré par l'Ifremer.

RÉSUME CONSOLIDE PUBLIC

B.1 RESUME CONSOLIDE PUBLIC EN FRANCAIS

L'objectif de la présente étude doctorale était de caractériser la sismicité en Mer de Marmara, aussi finement que possible, à partir des données enregistrées par un réseau de 10 Sismographes de Fond de Mer (OBS), déployés par Ifremer dans la zone de faille, entre avril et août 2011. Pour ce faire, nous avons utilisé des pointés manuels, ainsi qu'un modèle de très haute résolution (750 m x 750 m x 200 m) établi à partir de l'ensemble des données disponibles en Mer de Marmara. Une attention particulière a été portée sur une sequence de répliques faisant suite à un séisme de magnitude 5.2, survenu le 25 juillet 2011, au voisinage d'un volcan de boue, situé à moins d'un kilomètre de la zone de faille, sur la Haut Ouest. Les données montrent clairement que la sequence de répliques est avant tout constituée de séismes superficiels, situés entre 2 et 4 km sous le fond de la mer, dans la reservoir de gaz sous le haut ouest. Le système constitué par la zone de faille et le volcan de boue offre ainsi des chemins de migration au gaz, qui remonte du reservoir jusqu'à la surface. Nos résultats confirment l'intérêt du site (au voisinage du volcan de boue), pour le déploiement de futurs observatoires multi-paramètres.

L'étude post-doctorale préentée ici a été conduite par **Estelle Cros**, pendant 18 mois, du début avril 2012 à la fin septembre 2013. L'abondement Carnot a permis de co-financer le salaire d'Estelle pour une durée de 9 mois, ainsi que les frais correspondants (achat de materiel, PC, missions, participation à des colloques ou ateliers scientifiques, etc). Le reste du salaire a été assuré par l'Ifremer, après approbation de la commission *ad hoc* d'attribution des bourses post-doctorales. L'expérience acquise avec le présent post-doc a permis à l'Institut Carnot Ifremer-EDROME de développer des partenariats de recherche avec des groupes académiques (ISTERRE, IPG Strasbourg, IPG Paris, CEREGE), comme avec l'industrie (TOTAL). Un papier soumis en mai 2013 à *Marine Geophysical Researches* est en cours de révision. Un autre papier est en cours de preparation, pour soumission dans une revue à fort facteur d'impact en septembre 2015.

B.2 RESUME CONSOLIDE PUBLIC EN ANGLAIS

The main objective of the present post-doctoral study aims at improving the fine-scale characterization of earthquakes within the submerged section of the North-Anatolian fault, in the western part of Sea of Marmara, using the data recorded by a network of ten Ocean Bottom Seismometers (OBSs) deployed by Ifremer, between April and August, 2011. Manual picks on all individual OBSs were thus considered, in order to avoid artifacts resulting from LTA/STA algorithms. A high-resolution, 3D velocity model was used, with a node spacing of 750 m x 750 m x 200 m. Special focus was been given on the characterization of the aftershock sequence that followed the Mw 5.2 earthquake that occurred on July, 25th, 2011 on top of the Western High, in the area where gas hydrates are known to be present. We find that the aftershock sequence consists in well resolved epicenters located within the gas reservoir, 2 to 4 km below the mud volcano seafloor. The fault zone / mud volcano system clearly provides structures that convey gas to seeps at the seafloor. The gas follows migration pathways away from the fault zone, which at greater depth interact with the source of the gas. Our study clearly provides additional, new arguments that strongly support the implementation of multi-parameter observatories near the mud-volcano area on top of the Western High, in the search for transients.

The present 18-months long post-doctoral study presented here was co-funded by a double grant, from Ifremer and from institut Carnot respectively, to support the salary of **Estelle Cros** and the related expenses (computing facilities, travels). The experience gained during the present work will be used to develop new partnerships with academic groups (ISTERRE, IPG Strasbourg, IPG Paris, CEREGE) and with the industry (TOTAL). One paper was submitted to *Marine Geophysical Researches* in may 2013, and one paper is presently in preparation for submission to a *large impact factor journal* (september 2013).

MEMOIRE SCIENTIFIQUE

C.1 RESUME DU MEMOIRE

The Marmara Sea is located between the Agean Sea and the Black Sea, along the North Anatolian strike-slip fault, which experienced a sixty year sequence of earthquakes since 1940. Prior to this sequence, which ended with the Izmit and Duzce earthquakes in 1999, at the eastern end of the Sea of Marmara (SoM), the fault ruptured to the west in 1912 in Ganos, with an estimated moment magnitude of 7.4. Therefore, a major earthquake is expected within the SoM seismic gap.

In order to better understand the seismicity and to reduce the threshold of detection, a network of ten OBSs with four components was deployed by Ifremer, in the western and central parts of the Marmara Sea to record the micro-seismicity from the immediate vicinity of the main Marmara Fault, between April and August, 2011. The network was specifically designed to survey the segments crossing the Western High, where gas hydrates where recently found, the Central Basin and the Kumburgaz Basin. During this period about one hundred earthquakes were detected by the EMSC (European-Mediterranean Seismological Center) in the Sea of Marmara.

Because the basins of the Sea of Marmara are filled with more than 5 km of Plio-Quaternary soft ("slow") sediments, it is of critical importance to take into account the velocity structure of the offshore domain, which is drastically different from the one onshore, and the bathymetry. To improve the localization of seismic events, a high-resolution, 3D velocity model was thus considered, with a noe spacing of 750 m x 750 m x 200 m. Special focus was been given on the characterization of the aftershock sequence that followed the Mw 5.2 earthquake that occurred on July, 25th, 2011 on top of the Western High. A two-steps procedure: 1) absolute locations were first obtained using a 3D-velocity model and NLLOC, a non linear routine developed by Lomax [see references]; then, relative locations were obtained using HYPODD *[Waldhauser et al, 2000].*

We find that the aftershock sequence consists in well resolved epicenters located within the gas reservoir, 2 to 4 km below the mud volcano seafloor. The fault zone / mud volcano system clearly provides structures that convey gas to seeps at the seafloor. The gas follows migration pathways away from the fault zone, which at greater depth interact with the source of the gas. Hence, the physical properties and the chemistry of the fluids within the conduit of the mud volcano are likely to change systematically with the state of stress and strain in the fault zone throughout the earthquake cycle. Some of these changes, or their consequential effects, such as variations in gas emissions, could be recorded at the seafloor. Our study clearly provides additional, new arguments that strongly support the implementation of multi-parameter observatories near the mud-volcano area on top of the Western High, in the search for transients.

C.2 ENJEUX ET PROBLEMATIQUE, ETAT DE L'ART

The Sea of Marmara (SoM) is located between the Anatolian plate and the Eurasian plate (Figure 1a). The region is dominated by the right-lateral North Anatolian Fault (NAF) which accommodates most of the westward motion of the Eurasian plate, at a rate of ~25 mm/yr [Meade et al. 2002]. In the SoM the fault is splits into three separated branches called the Main Marmara Fault (MMF), the Southern branch and the Middle branch (Figure 1b).

During the last century, two earthquakes of magnitude of 7.3 and 7.4 occurred along this fault, in 1912 and 1999 respectively, and this region which is densely populated is menaced by the seismic activity of the NAF. Paleoseismological evidences tend to stop the rupture associated to the M_s 7.3 1912 Ganos earthquake in the west part of the SoM [Meghraoui,Aksoy,Akyuz,Ferry,Dikbas & Altunel 2012], while the M_s 7.4 1999 Izmit earthquake have ruptured fault segment situated 160 km away eastward. Relatively low strain is though to have been released by earthquakes since 1766 along the part of the NAF below the SoM, involving a seismic gap [Hubert-Ferrari et al. 2000; Meghraoui et al. 2012; Bohnhoff,Bulut,Dresen,Malin,Eken & Aktar 2013].

The deeper part of SoM is composed of three deep basins (respectively from east to west, the Çinarcik basin, the Central basin and the Tekirdag basin (Figure 1a)) filled with a thick layer of soft sediments [Laigle,Becel,de Voogd,Hirn,Taymaz & Ozalaybey 2008; Bécel et al. 2009; Bécel et al. 2010]. One of the main issue in the study of the seismicity in this area would then be to develop well adapted velocity model, especially to consider 3D velocity model to take into account the bathymetry of the sea. Recent studies on the seismicity in the SoM still used 1D velocity models [Karabulut et al. 2011; Örgülü 2011], but the tomographic velocity model of Bayrakci et al. [2013] will lead to carry out the location of the seismicity using 3D velocity models.

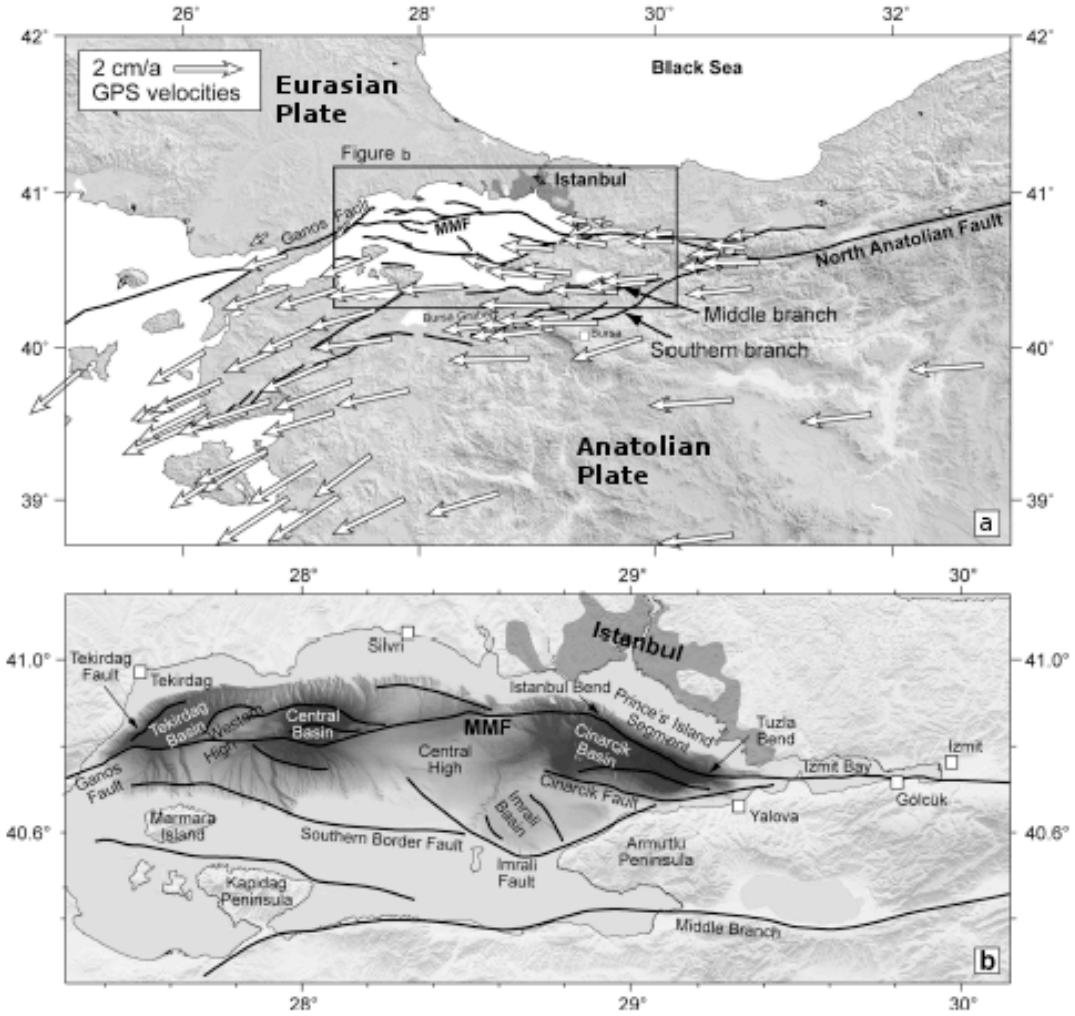

Figure 1: (a) GPS velocities in the area of the Northwest Anatolia. (b) Marmara Sea region and faults. Adapted from Hergert, Heidbach, Bécel and Laigle [2011].

C.3 APPROCHE SCIENTIFIQUE ET TECHNIQUE

C3.1 Travel time picking and Detection method

To monitor the fault segment of the NAF in the SoM, in 2011 a non-permanent network of ten 0BSs with four components was deployed (Figure 2) and recorded data during 107 days, from April 15th to July 31st (unfortunately OBS 2 failed and stopped recording after June 30th, 2011). The network was designed to complement the permanent submarine monitoring system of the Kandilli Observatory and Earthquake Research Institute (KOERI) and to carry out a high resolution characterization of earthquakes within the Western part of the SoM, including the Tekirdag basin, the Western High and the Central basin.

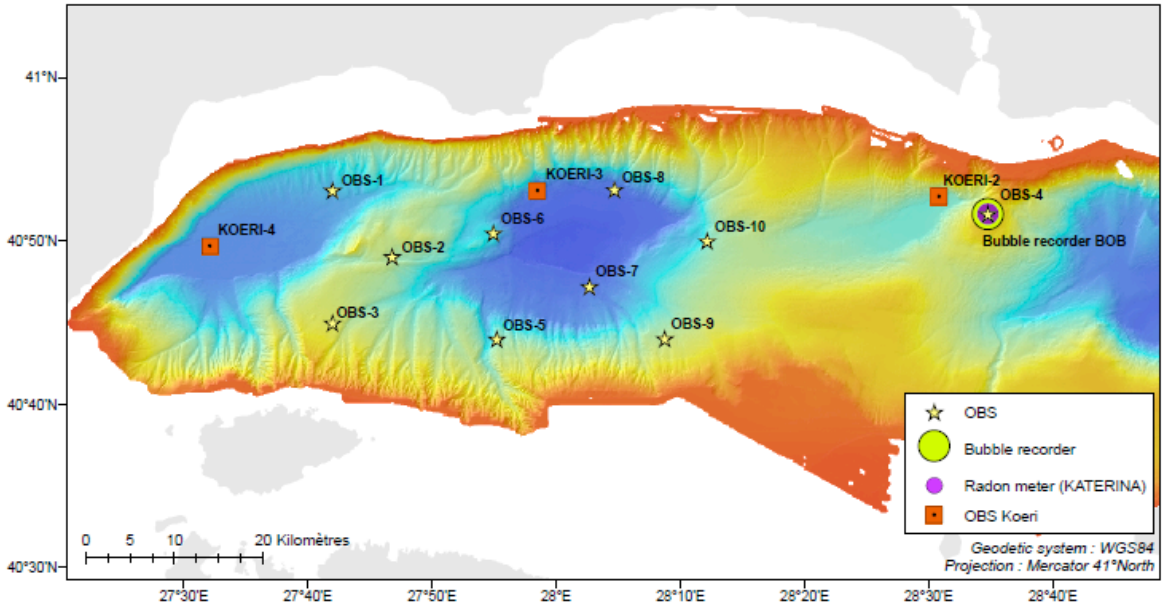

Figure 2: Bathymetric map of the Western and Central part of the Sea of Marmara. The study area is delineated by coordinates 40°43'N - 40°54'N – 27°30'E – 28°15'E (OBS 4 and KOERI 2 are not within this study area).

The first step of the study was to detect the seismic events. To do that, a STA/LTA algorithm was used through the Sytmis® software. The problem found was that electronic signals were also detected by the algorithm. Hence, the picking of the first arrivals was done manually and all this type of events were removed during this process. Almost 700 events were detected and picked manually (Figure 3), which represents a rate of 7 events by day. Most of the seismicity occurred during July 2011, with an amount of ~550 events. This high rate of seismicity is associated to a sequence of aftershocks that followed a Mw 5.2 earthquake, which occurred on July 25th at 17h57.

Manual picking on the OBS network proved to be very efficient to improve the detection threshold. For comparison: the catalog available on the website of the European-Mediterranean Seismological Center (EMSC) reports 145 events during the recording period, with only 70 in july 2011 (Figure 3). From this first observation we can underline the direct contribution of the proximity of the network to the fault which is the efficiency to detect a larger amount of seismic events.

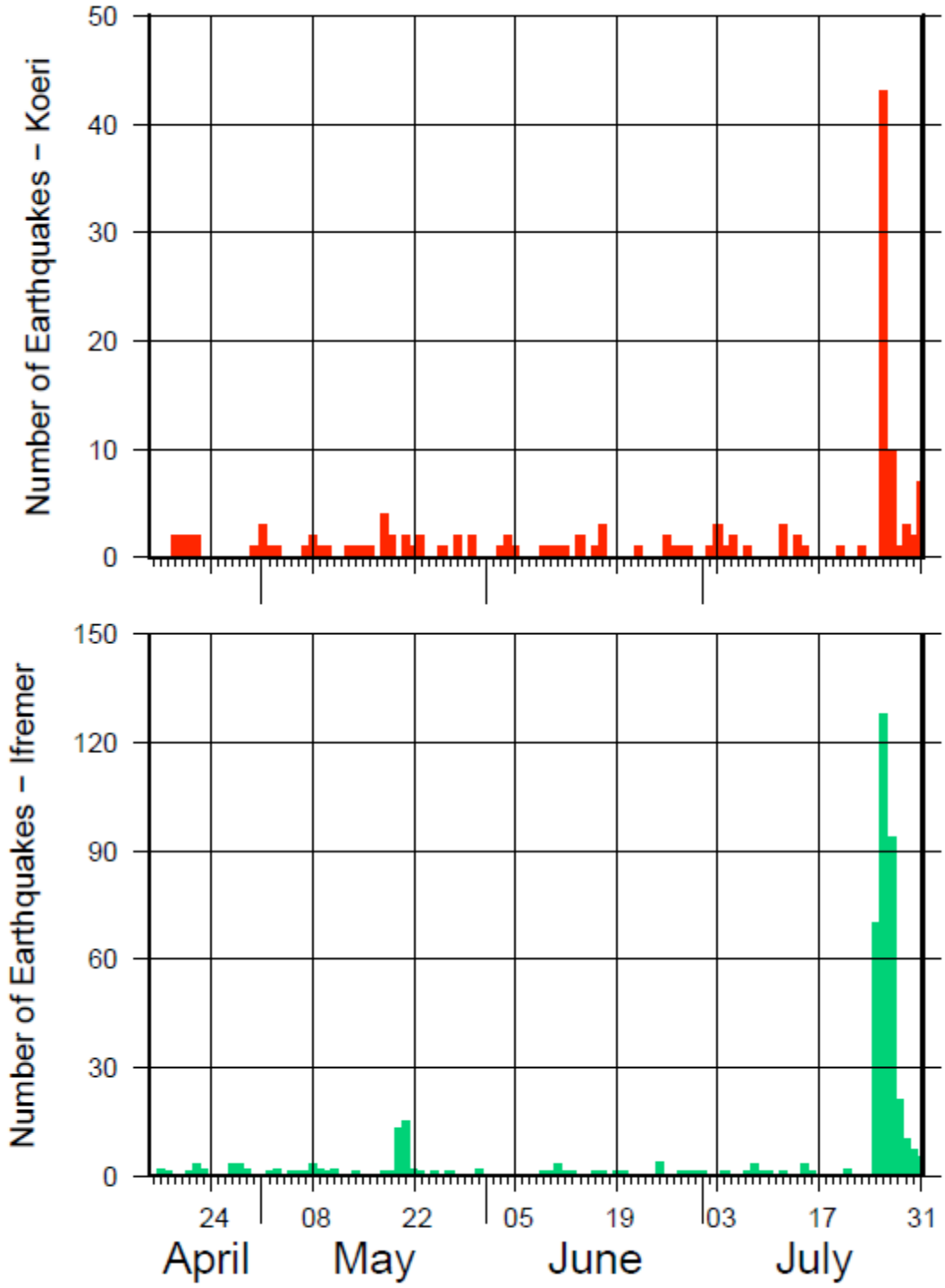

Figure 3: Number of events by day recorded on the catalog of the European-Mediterranean Seismological Center (EMSC) (top) and detected by the network of OBS (bottom).

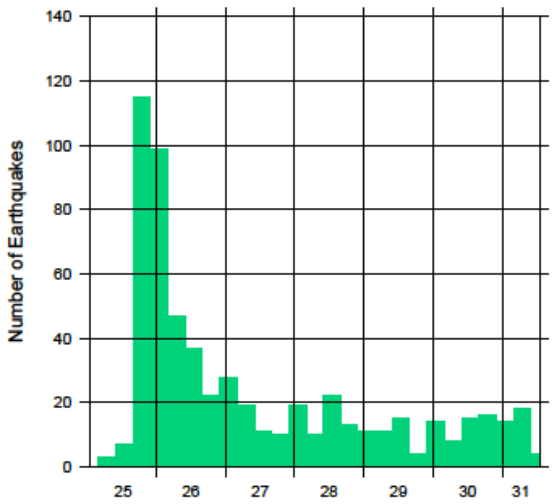

Figure 4: Histogram showing the number of events (over 6 hours periods) detected by the different OBSs, following the Mw 5.1 earthquake that occurred on July 25th, 2011, at 17:57. Almost half of the aftershocks occurred within the first 12 hours after the mainshock.

After picking the first arrivals, the next step was then to locate the earthquakes. A first analysis was carrying out using 1D velocity models that were implemented in the Sytmis® software. Four models were used (Figure 4):

- the model of Tary et al. [2011]
- a model based on Bécel [2006]
- the model of Gurbuz et al. [2000], and
- an average velocity model based on all these previous models.

The main difference between these models is the absence of a slow velocity layer in the top of the model calculated by Gurbuz et al. [2000]. In fact, the model derived by Gurbuz et al. [2000] is well adapted for on shore network. The model of Bécel [2006] is derived from sesimic refraction data from an East-West profil through the sea and the refraction model of the supracrustal part in the Central high.The 1D velocity model calculated by Tary et al. [2011] is a composite model based on high-resolution wide angle OBS data in the Tekirdag basin for the first 4km and for depth greater than 4km the seismic model in the Tekirdag calculated by Bécel [2006] was used. Finally, a smooth model composed of the three others models was calculated to combine the informations from the different 1D velocity models.

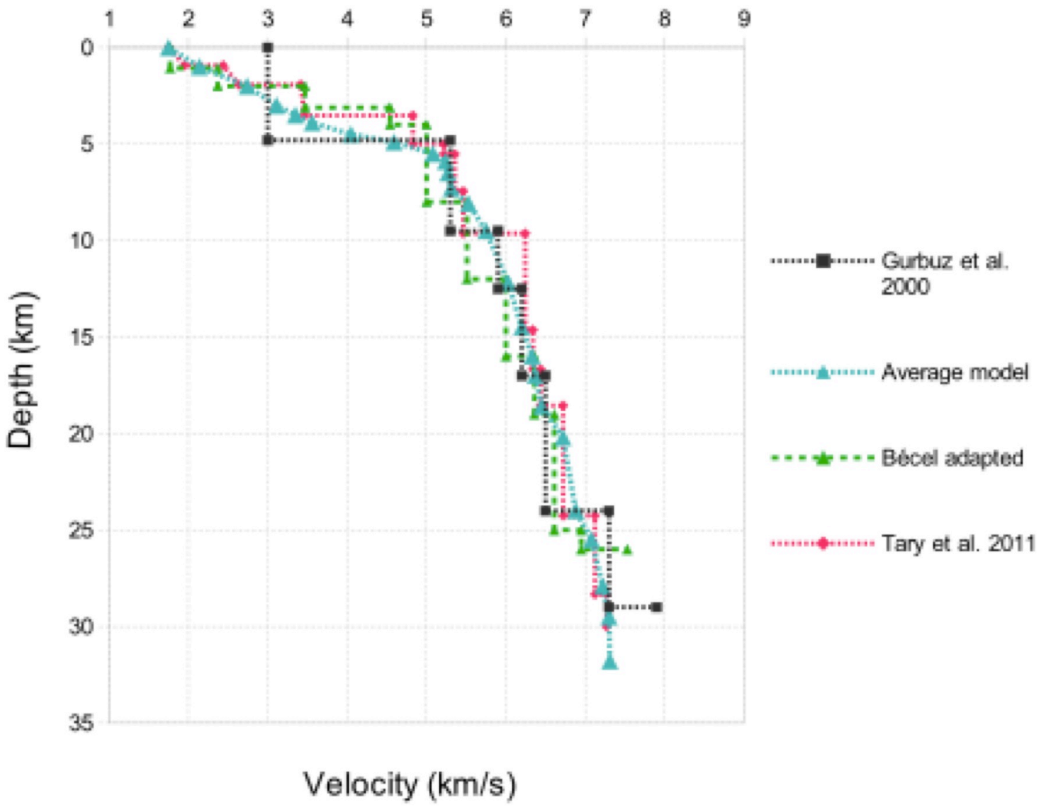

Fig. 5: 1-D velocity models used in the present study. In black the model of Gurbuz et al. [2000], in green the model of Bécel [2006],in red the model from Tary et al. [2011] and in blue a model calculated from the three others.

Locations calculated using these four different models allow us to select one model that was well adapted for this network and for the earthquakes detected within the recording record. The best results were obtained using the 1D velocity model of Tary et al. [2011]. This model was thus used hereafter, whenever a 1D model was necessary.

One dimensional models however do not account for the lateral variability of the bathymetry and velocity structure. To encompass the complexity in the velocity structure in the Sea of Marmara in the calculation of the location of the earthquakes, the software NLLOC was used using 3D velocity models.

The 3D tomographic model of Bayrakci et al. [2013] exhibits a grid spacing of 6km/6km/2km (Figure 5). The pre-kinematic basement (associated to a velocity of 4.2km/s) can be extracted from the model and is observed at a depth of 6.5 km for its deepest part in the Western high region. However, this model does not account for depths > 12 km and the grid spacing (6 km x 6 km x 2 km) is not appropriate high resolution earthquake characterization.

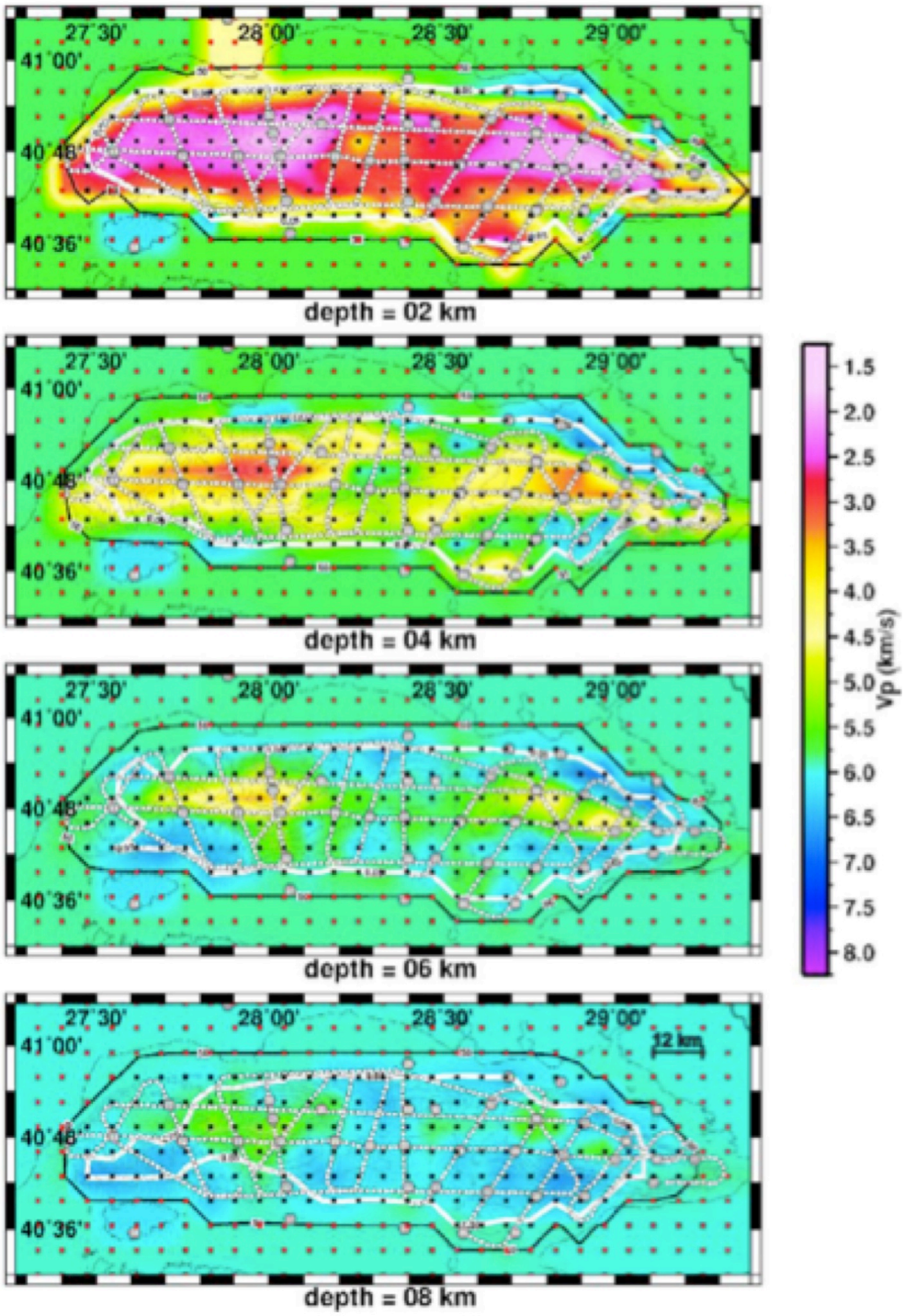

Fig. 6: After Bayrakci et al [2013]. Map view at 2, 4, 6 and 8 km depths of the inversion results. Grid node (black dots) spacing is 6 km x 6 km x 2 km. Grey hexagons are receivers (OBSs and land stations) of the survey. The white points are the considered shots. The white contour (RDE = 0.05) surrounds the well-resolved nodes identified by the checkerboard test. The black contour (DWS = 50) surrounds the nodes, which have been inverted during the inversion. The black crosses are the inverted nodes whereas the red ones are the fixed ones [Bayrakci et al. 2013].

C3.2 Choosing a specifically designed, fine-scale velocity model

In parallel to the study reported here, a complementary study was conducted within the EU-Funded MARSITE Project (www.marsite.eu), with among other targets, the objective to detect low magnitude earthquakes and improve the characterization of the near-fault micro-seismicity, particularly along the central part of the SoM. To meet this objective, velocity models were developed by KOERI and by Ifremer to improve earthquake location in the Sea of Marmara, following two different approaches:

- KOERI has developed a 3D velocity model for the whole Marmara Region (within latitudes 39.5°N - 42.5°N and longitudes 26.0°E - 30.5°E), including land and seabottom stations, with grid spacing of 9 km x 9 km x 3 km.

- Ifremer has developed a complementary approach, strictly based on seabottom stations, for the Western Sea of Marmara (40°43'N - 40°54'N – 27°30'E – 28°15'E). A high resolution velocity model with a 750 m x 750 m x 400 m grid spacing was built, using multibeam bathymetry and wide-angle seismic data, in order to account for the velocity contrast at the water/sediment interface and the slow seismic velocities within the sediment infill in the main Marmara Trough.

Because the objective of the present study is the high-resolution characterization of the afterhock sequence that followed the Mw 5.2 earthquake of July 25th, 2013, we here used the fine-scale 3D-velocity model developed by Ifremer for the western Sea of Marmara. This model was elaborated, following the six steps hereafter described:

1. The initial tomographic model of Bayrakci et al. [2013] (6 km x 6 km x 2 km) was used as initial model to describe the velocity structure of the pre-kinematic basement and the velocity structure down to 12km depth below sea level.
2. The iso-depth contours of the pre-kinematic basement were used as guide lines to define 9 domains for the study area (Figure 7), having each a "typical" velocity profile down to 12 km depth. Each "typical " profile corresponds to an average curve calculated at 5 different depths (0-2-4-6-8 km depth). For instance, for one domain, the value at 4 km depth corresponds to the mean of values at 4 km for all points constituting this domain.
3. A dense, high-resolution sub-grid was then defined for the study area (Figure 8), with grid spacing 750 m x 750 m x 200 m, by sub-dividing the tomographic grid of Bayrakci et al. [2013] (6 km = 8 x 750m).
4. Each node M of the dense sub-grid was ascribed: to: i) the water depth inferred from the high resolution bathymetric grid of Le Pichon et al. [2001]; ii) to a given domain N (with N=1 to 9, as defined in Figure 7). The velocity structure at grid node M for the upper 12 km is provided by the characteristic velocity profile of domain N.
5. Below 12 km and down to 36 km, the velocity structure is assumed to depend on longitude and inferred from the Wide-Angle Reflexion results of Bécel et al. [2009]. Velocities of 6.7 km/s and 8 km/s were ascribed to the lower crust and upper mantle respectively.
6. Each point of the fine sub-grid is thus characterized by : depth, "domain" number, "typical" velocity profile above 12 km, depth of lower crust, depth of Moho.

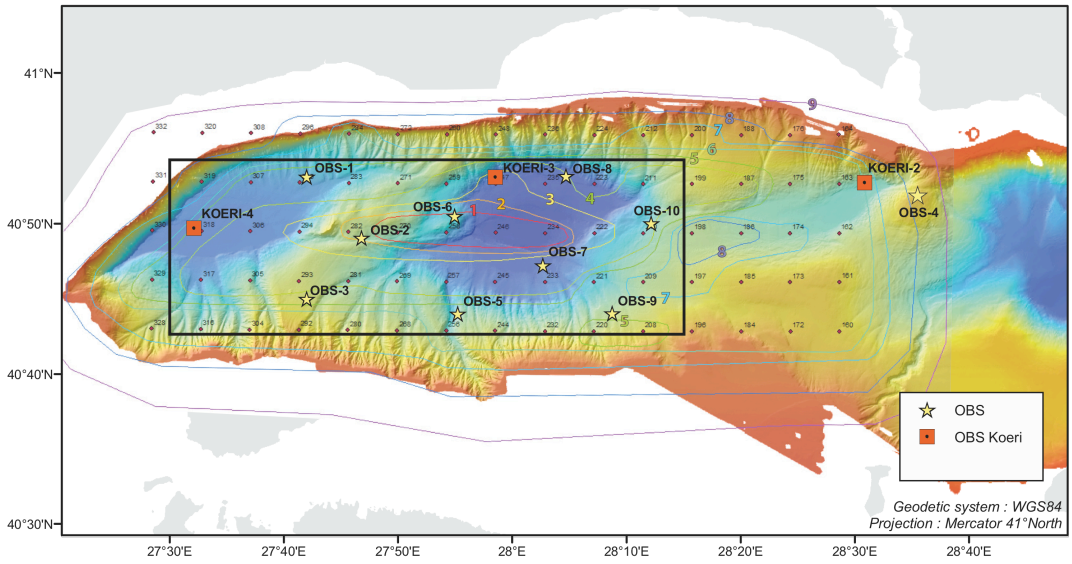

Figure 7a: Bathymetric map of the western the Sea of Marmara, with dots indicating grid nodes (with 6 km x 6 km spacing) from the tomographic model of Bayrakci et al. [2013]. Colour lines are based on iso-depth contours of the pre-kinematic basement inferred from the tomographic model (Figure 6). These contour lines are used here to delineate 9 domains having a characteristic velocity structure in the upper 12 kilometers. Domain 1 is delineated by contour 1. Domain N is between contours N-1 and N (N=2 to 9).

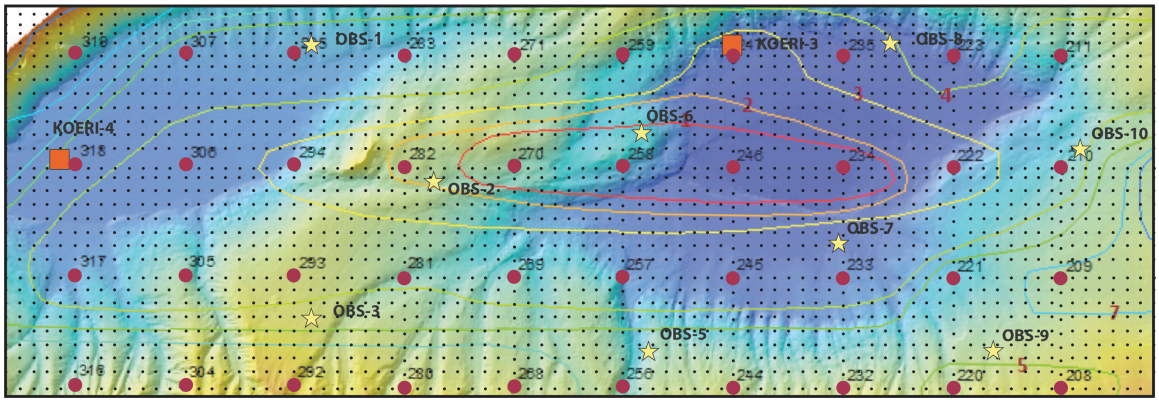

Figure 7b: Final grid nodes (with node spacing of 750 m x 750 x 200 m) used in the present study for the high-resolution characterization of earthquakes in the Western Sea of Marmara. Numbers indicate grid nodes from Bayrakci et al. [2013]. Each final grid node M is ascribed to: i) the water depth inferred from the high resolution bathymetric grid of Le Pichon et al. [2001] ; ii) to a given domain N (with N=1 to 9, see Figure 7). The velocity structure at grid node M for the upper 12 km is provided by the characteristic velocity profile of domain N. Below 12 km, the velocity structure is assumed to depend on longitude and inferred from the Wide-Angle Reflexion results of Bécel et al. [2009].

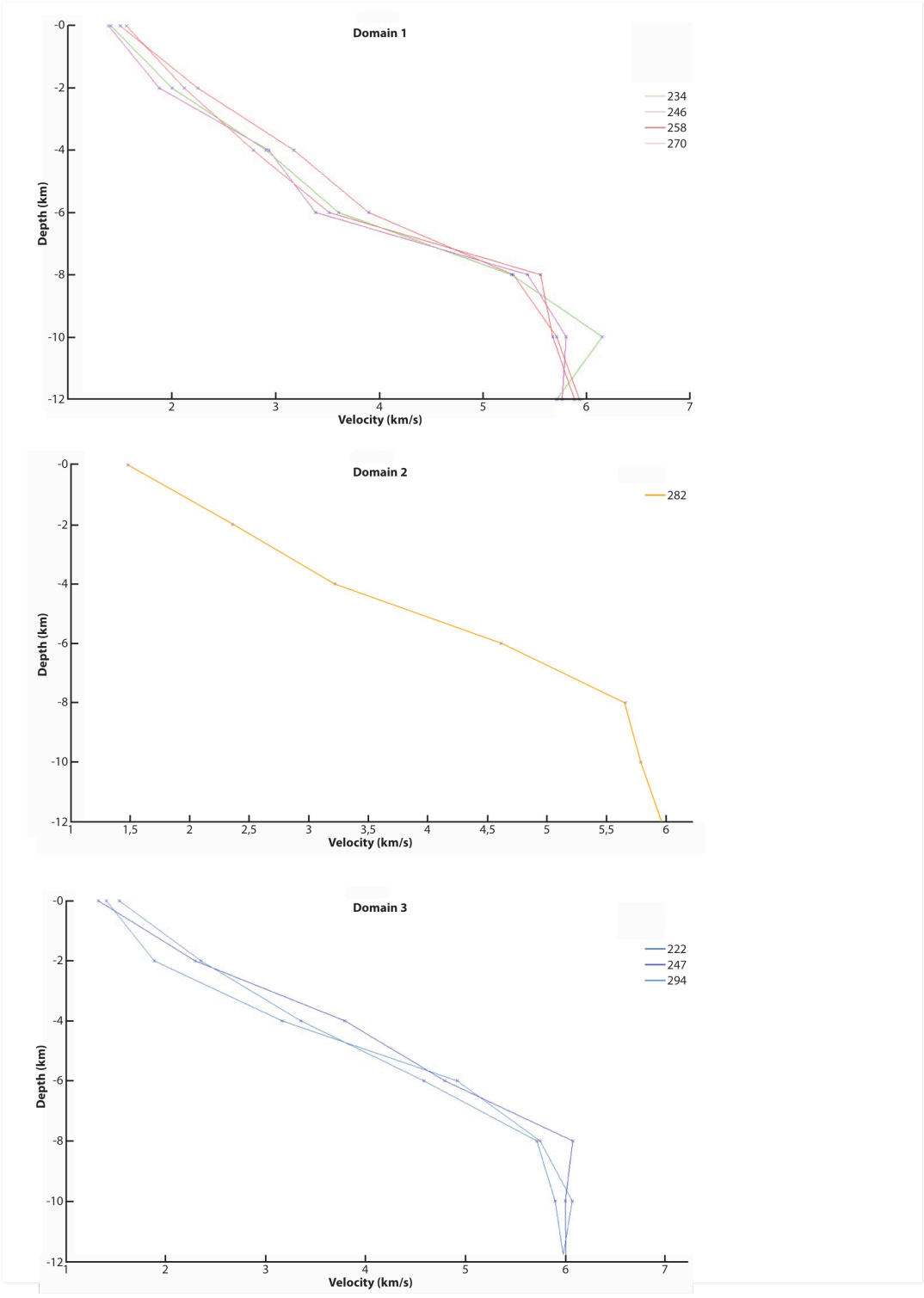

Figure 8a: Vertical velocity profiles (from 0 to 12 km depth below seafloor) below each node of the low-resolution, tomographic grid of Bayrakci et al [2013], within, respectively domains 1, 2 and 3 (see domain delineation in Figure A2-1).

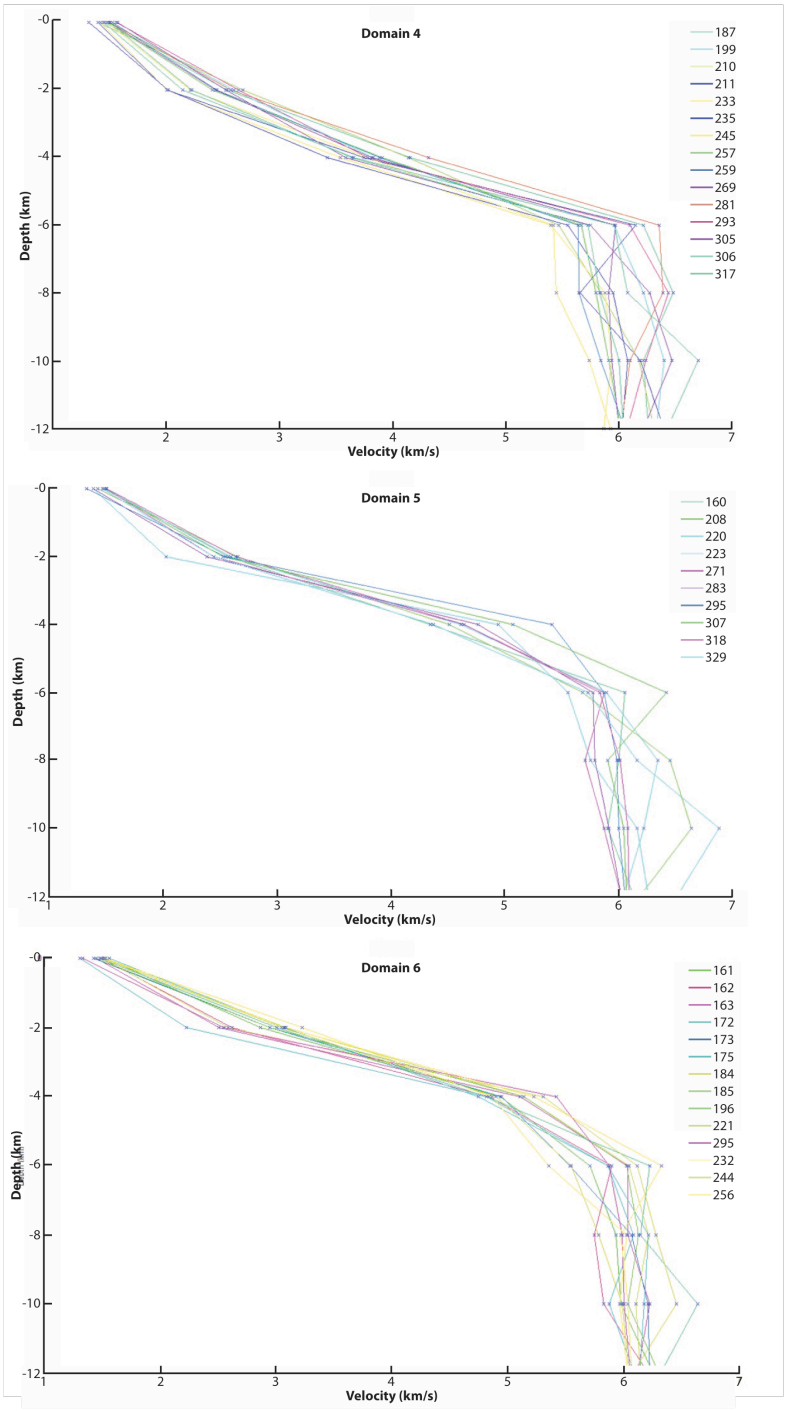

Figure 8b: Vertical velocity profiles (from 0 to 12 km depth below seafloor) below each node of the low-resolution, tomographic grid of Bayrakci et al [2013], within, respectively domains 4, 5 and 6 (see domain delineation in Figure A2-1).

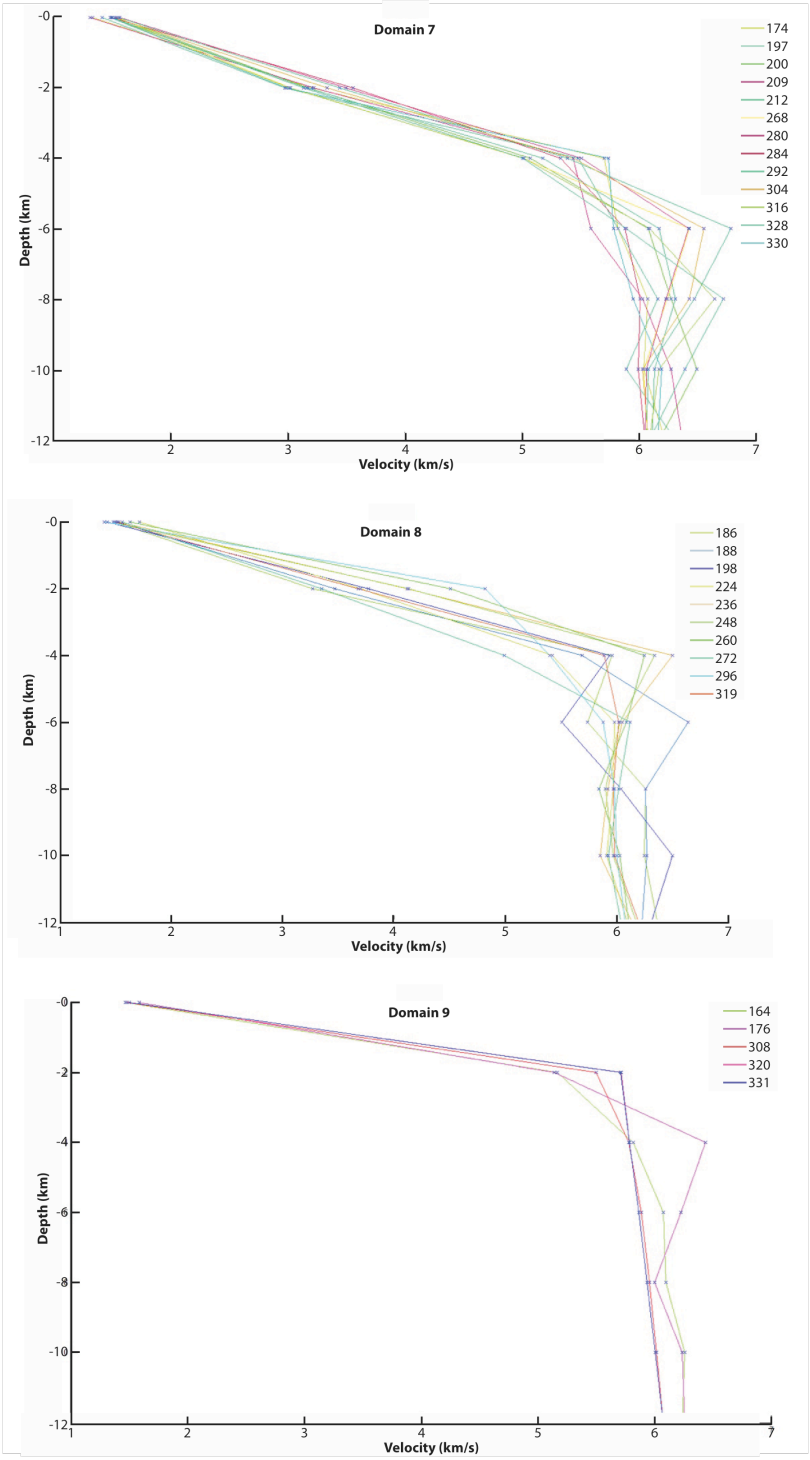

Figure 8c: Vertical velocity profiles (from 0 to 12 km depth below seafloor) below each node of the low-resolution, tomographic grid of Bayrakci et al [2013], within, respectively domains 7, 8 and 9 (see domain delineation in Figure A2-1).

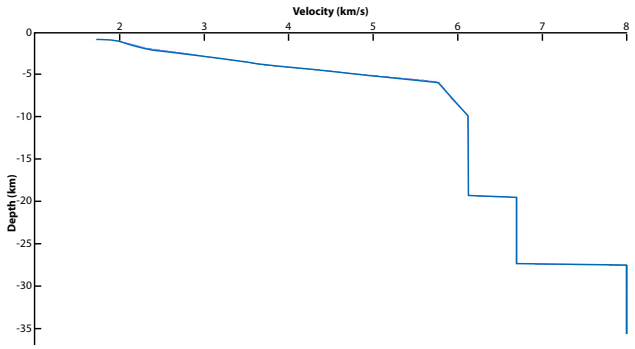

Figure 9: Example of velocity profile finally obtained for node located within domain 4, at longitude 27°37.56'E, latitude 40°46.50'N. The typical velocity profile of domain 4 is used for z < 12 km. For z > 12 km, velocities and interface depth for lower Crust and Moho depth are inferred as a function of longitude, based on wide-angle and refraction seismics results (e.g. see Figure 10 of Bécel et al [2009]).

C.4 RESULTATS OBTENUS

This section strictly focuses on the fine characterization of the 3-days long aftershock sequence that followed the Mw 5.1 earthquake which occured on July, 25th, 2011, at 17h57 (Fig. 9). The fine scale characterization was obtained following a two-steps procedure: 1) absolute locations were first obtained using a 3D-velocity model and NLLOC, a non linear routine developed by Lomax [see references]; then, relative locations were obtained using HYPODD *[Waldhauser et al, 2000]* and the 1-D velocity model of *Tary et al. [2011].*

Locations using the 6 km x 6 km x 2 km 3D-velocity model of Bayrakci et al [2013] (Figs. 10 to 12). Absolute locations are evenly distributed between the sea-floor and 15 km at depth, with most of the seismicity concentrated on the Western High (Figure 10 top). Still, many aftershocks are located away from the mainshock and delineate an E-W trend below the Tekirdag Basin. Relative localization using HypoDD strongly reduces the RMS and focuses the seismicity along the fault on top of the Western High. Still, many events are found in the Tekirdag Basin along the same E-W trend (Figure 10 middle). In the vertical section (Figure 10 bottom), relative locations appear distributed into 2 groups of events, between the sea-floor and 6 km depth, and between 6 and 12 km depth, respectively.

In order to eliminate possible artifacts related to the uneven distribution of OBSs, we considered a specific sub-network defined by 4 stations symmetrically distributed on a circle more or less centered on the mainshock: 3 IFREMER OBSs *(OBS1*, *OBS6* and *OBS3)*, and one KOERI station *(KOERI4*). Only those events having arrivals picks on the 4 OBSs were considered. Using the 3D velocity model of Bayrakci et al. [2013], most absolute locations appear to be mostly focused on the Western High and located at a depth above 15 km (Figure 12 top). Relative localization using HypoDD results in improved focusing above the Western High and shallower events (depth < 10 km). Interestingly, two groups of earthquakes appear: one with depths between 0 and 5 km; and one with depths between 8 and 14 km.

Locations using the Bayrakci-Coutellier-Cros 3D-velocity model with grid mesh size of 1500 m x 1500 m x 400 m (BCC-1 model) (Figs. 13 and 14). Absolute locations are dispersed within the Tekirdag Basin, with E-W trends (Fig. 13 top). Relative locations obtained with HypoDD are more focused near the epicenter of the mainshock (Fig. 13 middle) and shallower (Fig. 13 bottom) than with the Bayrakci's model.

Absolute and relative locations obtained with the BCC-1 model and picks from the sub-network only, appear to be much more focused and closer from the fault (Figure 14 top and middle) than those obtained with the Bayrakci et al. [2013] model (Figure 12 top and middle). Interestingly, two different groups of events clearly appear: one with relative location depths between 0 and 5 km; and one with relative location depths between 8 and 14 km (Fig. 14).

Location using the Bayrakci-Coutellier-Cros 3D-velocity model with grid mesh size of 750 m x 750 m x 200 m (BCC-2 model) (Fig. 15 and 16). The general trends described above (with BCC-1 model) are enhanced when using the BBC-2 model. Absolute locations are dispersed within the Tekirdag Basin, with E-W trends (Fig. 15 top). Relative locations obtained with HypoDD are more focused near the epicenter of the mainshock (Fig. 15 middle) and shallower (Fig. 15 bottom) than with the Bayrakci's or the BCC-1 model.

Both absolute and relative locations obtained with the BCC-2 model and picks from the sub-network only, appear to be much more focused and closer from the fault (Figure 16 top and middle) than those obtained with the Bayrakci et al. [2013] and BCC-1 models (respectively Fig. 12 and 14, top and middle). Again, two different groups of events clearly appear: one with relative location depths between 0 and 5 km; and one with relative location depths between 8 and 14 km (Fig. 16 bottom to be compared with Fig. 14 bottom and Fig. 12 bottom).

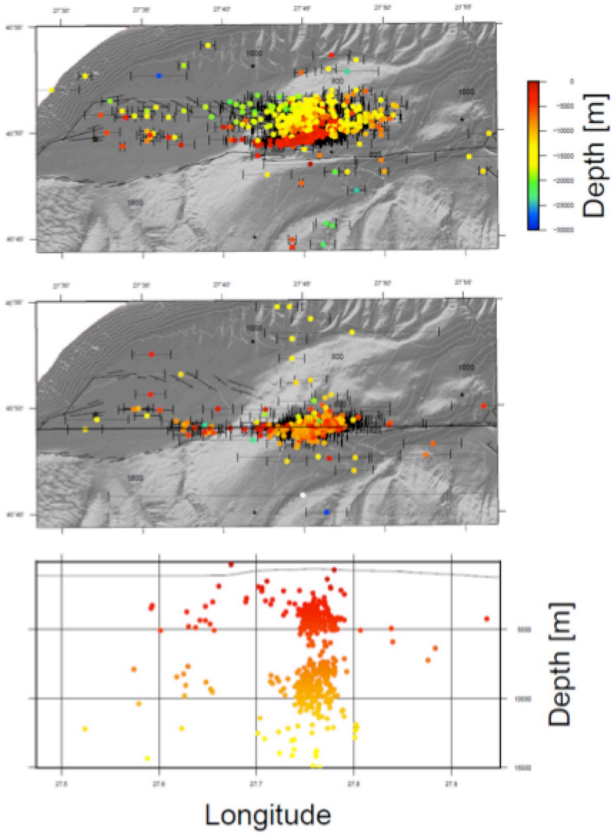

Fig. 10 Top : Absolute locations of aftershocks using the 3D velocity model of Bayrakci et al. [2013] and NLLOC developed by Anthony Lomax. Middle : relative locations using the 1D velocity model of Tary et al. [2011] and hypoDD [Waldhauser et al, 2000]. Bottom : Vertical cross-section showing depth distribution of epicenters (relative locations).

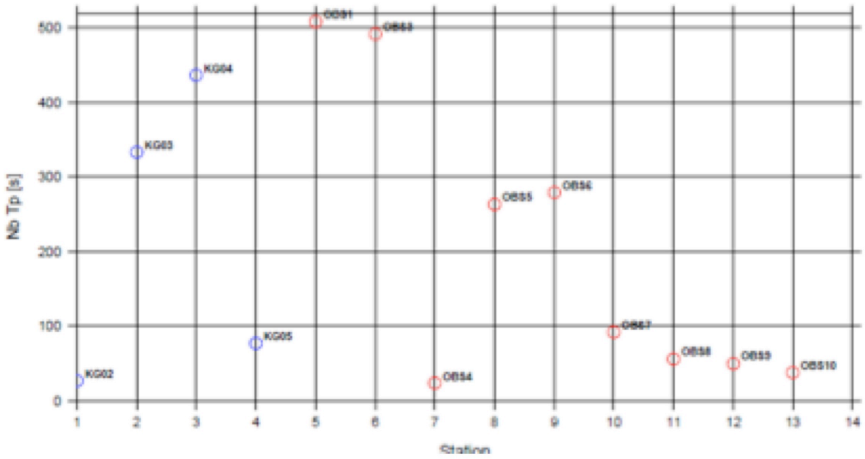

Fig. 11 Number of picks detected at each OBS (IFREMER and KOERI)

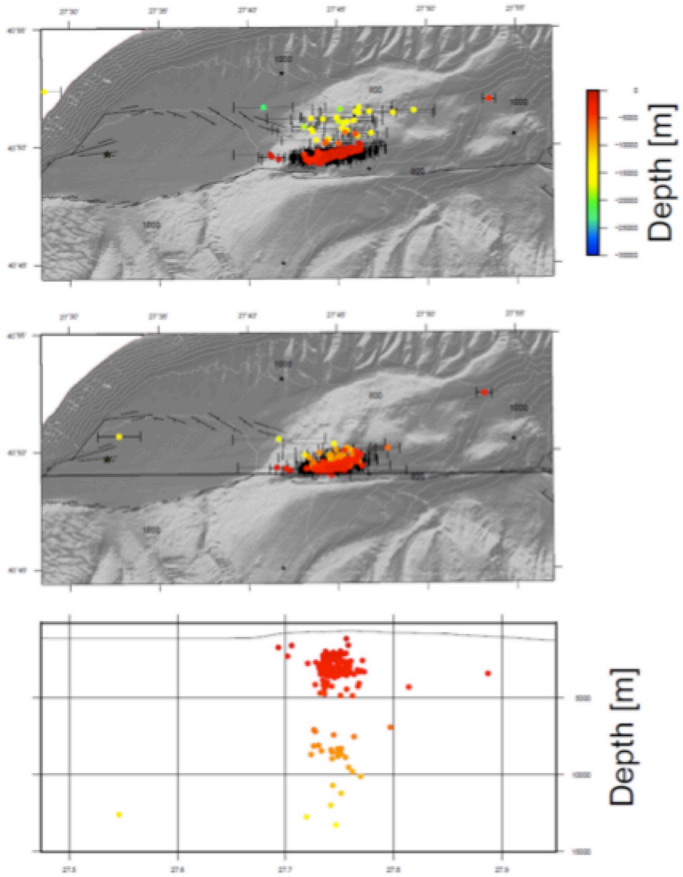

Fig. 12 In order to eliminate possible artifacts related to the uneven distribution of OBSs, we considered a specific sub-network defined by 4 stations symmetrically distributed on a circle more or less centered on the mainshock : 3 IFREMER OBSs (OBS1, OBS6 and OBS3), and one KOERI station (KOERI4). Only those events having arrivals picks on the 4 OBSs are here considered in the present figure. Top : Absolute locations of aftershocks using the 3D velocity model of Bayrakci et al. [2013] and NLLOC developed by Anthony Lomax. Middle : relative locations using the 1D velocity model of Tary et al. [2011] and hypoDD [Waldhauser et al, 2000]. Bottom : Vertical cross-section showing depth distribution of epicenters (relative locations).

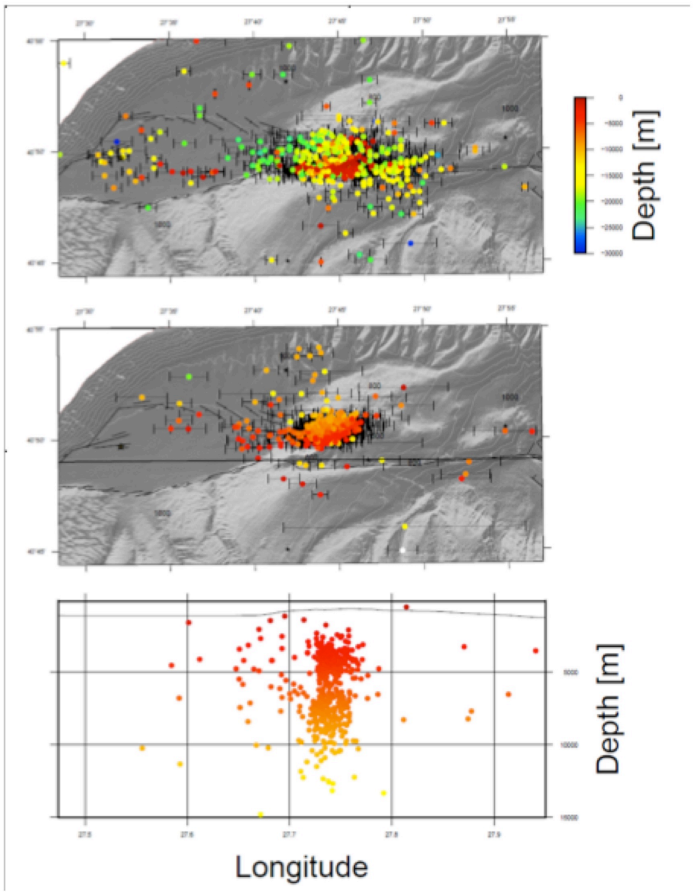

Fig. 13 Top : Absolute locations of aftershocks using the BCC-1, 3D velocity model (1.5 km x 1.5 km x 0.4 km) and NLLOC developed by Anthony Lomax. Middle : relative locations using the 1D velocity model of Tary et al. [2011] and hypoDD [Waldhauser et al, 2000]. Bottom : Vertical cross-section showing depth distribution of epicenters (relative locations).

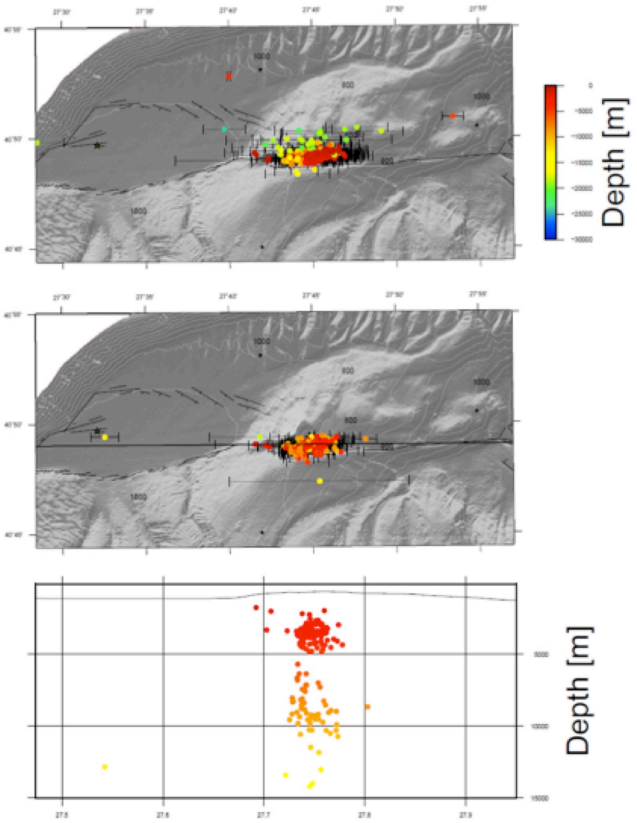

Fig. 14 In order to eliminate possible artifacts related to the uneven distribution of OBSs, we considered a specific sub-network defined by 4 stations symmetrically distributed on a circle more or less centered on the mainshock : 3 IFREMER OBSs (OBS1, OBS6 and OBS3), and one KOERI station (KOERI4). Only those events having arrivals picks on the 4 OBSs are here considered in the present figure. Top : Absolute locations of aftershocks using the BCC-1, 3D velocity model (1.5 km x 1.5 km x 0.4 km) and NLLOC developed by Anthony Lomax. Middle : relative locations using the 1D velocity model of Tary et al. [2011] and hypoDD [Waldhauser et al, 2000]. Bottom : Vertical cross-section showing depth distribution of epicenters (relative locations).

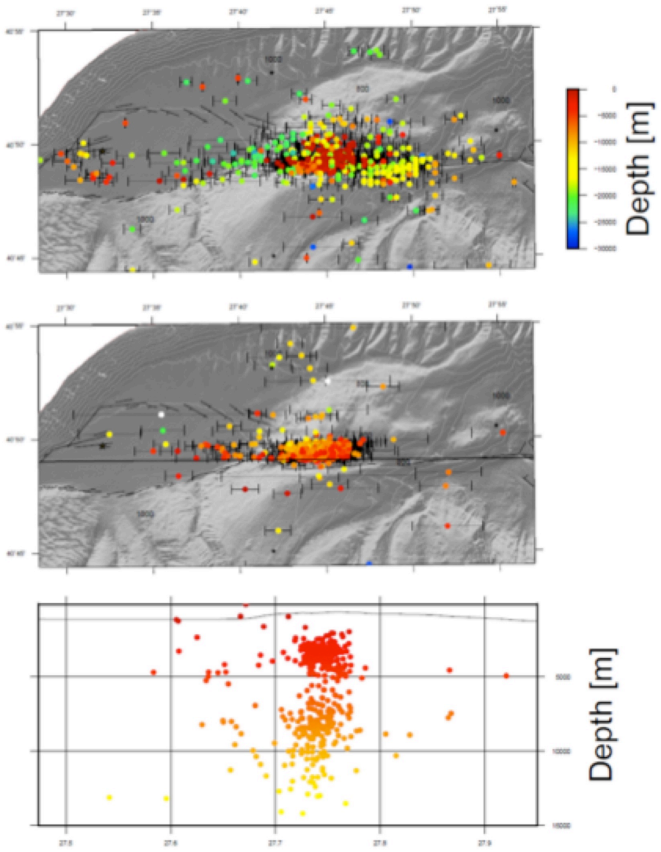

Fig. 15 Top : Absolute locations of aftershocks using the BCC-2, 3D velocity model (750 m x 750 m x 200 m) and NLLOC developed by Anthony Lomax. Middle : relative locations using the 1D velocity model of Tary et al. [2011] and hypoDD [Waldhauser et al, 2000]. Bottom : Vertical cross-section showing depth distribution of epicenters (relative locations).

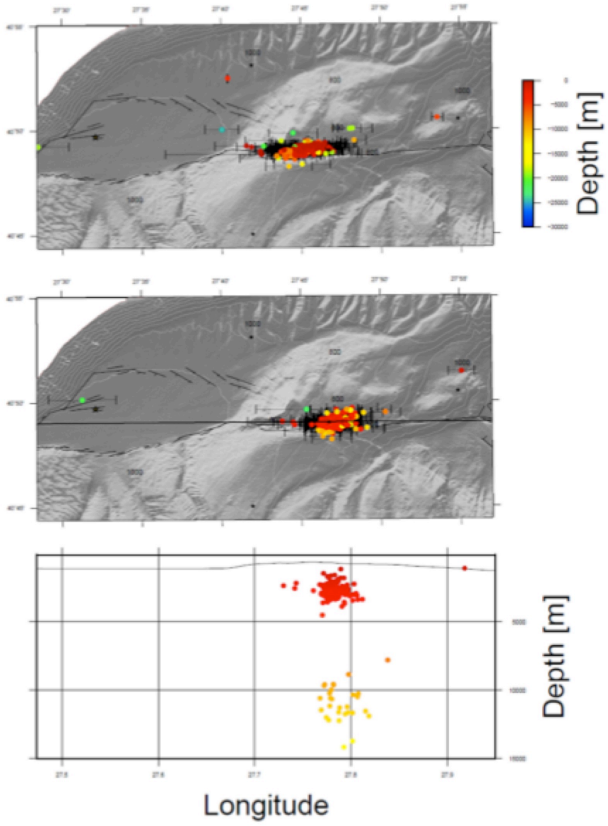

Fig. 16 In order to eliminate possible artifacts related to the uneven distribution of OBSs, we considered a specific sub-network defined by 4 stations symmetrically distributed on a circle more or less centered on the mainshock : 3 IFREMER OBSs (OBS1, OBS6 and OBS3), and one KOERI station (KOERI4). Only those events having arrivals picks on the 4 OBSs are here considered in the present figure. Top : Absolute locations of aftershocks using the BCC-2, 3D velocity model (750 m x 750 m x 200 m) and NLLOC developed by Anthony Lomax. Middle : relative locations using the 1D velocity model of Tary et al. [2011] and hypoDD [Waldhauser et al, 2000]. Bottom : Vertical cross-section showing depth distribution of epicenters (relative locations).

C.5 EXPLOITATION DES RESULTATS

The search for fluid-related, non-seismic transients during the stress building process at active faults is recognized by part of the scientific community as a major challenge for earthquake prediction research. A critical obstacle, though, is that even if such transients do exist, they are generally recorded at the surface and the relation to variations in stress and strain within the seismogenic zone is difficult, if not impossible, to establish. It has been recently discovered that thermogenic gas is emitted from seabed seeps in the proximity of the North Anatolian Fault within the western part of Sea of Marmara. High-resolution, 3D seismic data from where the North Anatolian Fault cuts a gas / oil system from the Thrace Basin province, show a diapiric feature that pierces the crest of an anticline, within less than 1 km of the fault zone. Based on new heat flow data and on published geochemical information, the gas prone layer is located at depths greater than ~ 2 km below seafloor, well into the seismogenic zone.

On July 25th, 2011, an earthquake of magnitude Mw 5.2 earthquake occurred in the near vicinity of the mud volcano. In the present study, based on a well distributed OBS network, we show that this earthquake was followed by a 3-days long aftershock sequence, with well resolved epicenters located within the gas reservoir, 2 to 4 km below the mud volcano seafloor. The fault zone / mud volcano system clearly provides structures that convey gas to seeps at the seafloor. The gas follows migration pathways away from the fault zone, which at greater depth interact with the source of the gas. Hence, the physical properties and the chemistry of the fluids within the conduit of the mud volcano are likely to change systematically with the state of stress and strain in the fault zone throughout the earthquake cycle. Some of these changes, or their consequential effects, such as variations in gas emissions, could be recorded at the seafloor. Our study clearly provides additional, new arguments that strongly support the implementation of multi-parameter observatories near the mud-volcano area on top of the Western High, in the search for transients. If seismic tremors are found to be associated with clear anomalies in gas emission activity, then we will have more criteria for characterizing and identifying the recorded signals as indicators that the probability of occurrence of an impending earthquake is increasing.

C.6 DISCUSSION

In Section C4, we have located well resolved, shallow aftershocks at depths ranging between 2 and 4 km below seafloor, using manually picked travel-times, a high-resolution velocity model and a well balanced network of 4 OBSs centered on the epicenter of the Mw 5.2 earthquake. The results are here compared to those obtained by our Turkish colleagues from KOERI within the MARSITE Project (www.marsite.eu), who have followed a very different approach, by developing a 3D velocity model for the whole Marmara Region (within latitudes 39.5°N - 42.5°N and longitudes 26.0°E - 30.5°E), including land and seabottom stations, with grid spacing of 9 km x 9 km x 3 km : see in *[Gürbüz et al, 2013]* and in *[Isik, 2014].* The data consist in first arrival times detected from seismograms generated by earthquakes that occurred between October 1st, 2009 and December 31st, 2012, over a large area encompassing part of the Black Sea, the Eastern Marmara and Thrace Regions (26°E-30.5°E – 39.5°N-42.5°N), so as to increase the number of earthquakes and improve the resolution on land. The travel times were recorded by 98 permanent, land stations and by 5 permanent, cabled, seabottom stations, operated by KOERI. In addition the following data were used to derive the 3D velocity model: i) Ifremer OBS data, recorded during 2 limited time windows (from October 1st, 2009 to March 15th, 2010, and from April 15th, 2011 to July 31st, 2011); ii) seismic data, from shots produced by R/V Nadir during the Seismarmara cruise in 2001.

The sequence that followed the Mw 5.2 earthquake was located using mostly the OBS that were deployed at that time: KOERI's cabled network of submarine stations and Ifremer OBSs. The major differences between our absolute locations (Fig. 15 and 16) and KOERI's (Fig. 18) are thus mainly due to differences in the velocity models. Merging land and sea-bottom datasets hence appears to be very challenging, if not hopeless, for the fine-scale characterization of seismicity within the fault zone.

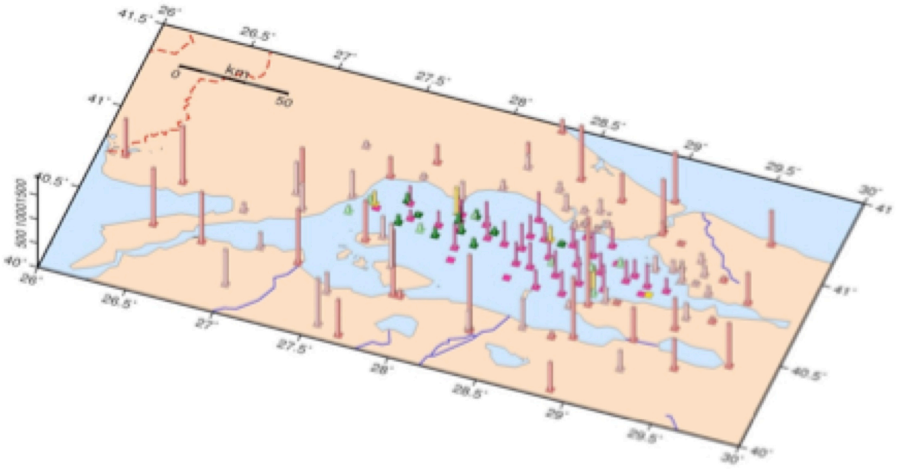

Fig. 17: Number of recordings per station used by KOERI to derive the large scale velocity model for the whole Marmara region. The number of recordings at stations located north of the Marmara Sea is remarkably less than those located to the south. Also, light green (FR) and dark green stations (FR) have less recordings compared to those on land. However, the pink stations which recorded the shots provide a good ray coverage with dense data. The light pink stations of TUBITAK fill the gap around the Marmara Sea but with less data then KOERI stations on land. Light orange stations of KOERI located at the outer boundary of the study area have the largest amount of recordings.

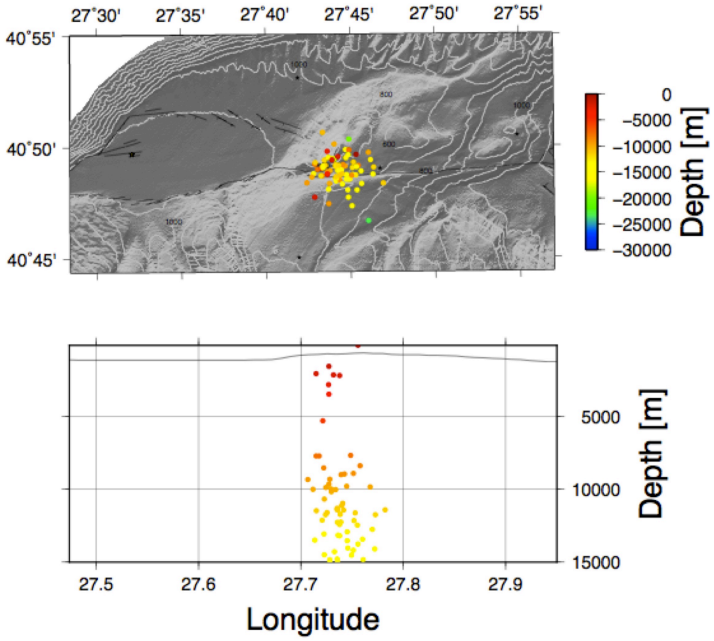

Fig. 18: Absolute locations of the aftershock sequence that followed the Mw 5.2 earthquake of July, 25th, 2011. Absolute locations were obtained by Cemil Gürbüz and colleagues from KOERI, using the KOERI's large-scale model, with a node spacing of 9 km x 9 km x 3 km. Most of the picks that were used for the location were recorded with seabottom stations including Ifremer OBSs and KOERI's permanent, cabled observatories. Compare with Figure15 and 16.

C.7 CONCLUSIONS

Because the basins of the Sea of Marmara are filled with more than 5 km of Plio-Quaternary soft ("slow") sediments, the velocity structure of the offshore domain is drastically different from the one onshore. Travel times are strongly controlled by: i) the sea bottom topography and the velocity contrast at the water/sediment interface; ii) the slow seismic velocities within the sediment infill in the main Marmara Trough:

- Large-scale velocity models for the whole Marmara region obtained by merging land and sea stations may prove to be very useful to improve the quality of earthquake catalogs and the real time monitoring of the regional seismicity.

- In contrast, to improve the final-scale location of hypocenters near the submerged fault zone and enhance the search for seismic tremors [*Bouchon et al.,* 2011], specific networks of permanent, cabled sea-bottom seismometers are required. Each network should be consistent *per se*, and allow the high-resolution characterization of earthquakes below the Sea of Marmara. In addition, it is of critical importance to create an high-resolution, 3D velocity model, in order to take into account for the velocity contrast at the water/sediment interface and the slow seismic velocities within the sediment infill in the main Marmara Trough.

- In the present study, a high-resolution, 3D velocity model was used for a 20 km x 60 km area located in the Western Sea of Marmara (750 m x 750 m x 430 m grid spacing). The seabottom topography was derived from a high-resolution grid (38 m) based on mulitbeam bathymetric data collected in 2000 *[Le Pichon et al., 2001]. Th*e structure of the sediment basin was determined using: i) the 3D tomographic model of *[Bayracki et al., 2013]*; ii) velocity models along 2D, wide-angle seismics lines *[Bécel et al., 2010*]; iii) all the geological information from the Marmara Sea resulting from the numerous cruises that have been carried out the Sea of Marmara since 1999*.*

- Using i) the above high-resolution velocity model, ii) a well distributed network of 4 OBSs centered on the mud volcano, and iii) manually picked travel-times, we show that the majority of aftershocks that followed the Mw 5.2 earthquake of July 25th, 2011, are located in a gas prone reservoir, 2 to 4 km below seafloor.

- The results confirm that the mud volcano area, on top of the Western High, is particularly adapted for implementing a multi-parameter observatory in the Sea of Marmara.

C.8 REFERENCES

Bécel, A. (2006). *Structure sismique de la Faille Nord Anatolienne en Mer de Marmara*, Université Denis Diderot.

Bécel, A.; Laigle, M.; de Voogd, B.; Hirn, A.; Taymaz, T.; Galvé, A.; Shimamura, H.; Murai, Y.; Lépine, J.-C.; Sapin, M. & Özalaybey, S. (2009). Moho, crustal architecture and deep deformation under the North Marmara Trough, from the SEISMARMARA Leg 1 offshore-onshore reflection-refraction survey, *Tectonophysics* **467**: 1-21.

Bécel, A.; Laigle, M.; de Voogd, B.; Hirn, A.; Taymaz, T.; Yolsal-Cevikbilen, S. & Shimamura, H. (2010). North Marmara Trough architecture of basin infill, basement and faults, from PSDM reflection and OBS refraction seismics, *Tectonophysics* **490** : 1-14.

Bayrakci, G.; Laigle, M.; Bécel, A.; Hirn, A.; Taymaz, T.; Yolsal-Cevikbilen, S. & team, S. (2013). *3-D sediment-basement tomography of the Northern Marmara trough by a dense OBS network at the nodes of a grid of controlled source profiles along the North Anatolian fault*, *Geophys. J. Int*. **194** : 1335-1357

Bohnhoff, M.; Bulut, F.; Dresen, G.; Malin, P. E.; Eken, T. & Aktar, M. (2013). *An earthquake gap south of Istanbul*, *Nat Commun*. **4** : -.

Gürbüz, C.; Aktar, M.; Eyidogan, H.; Cisternas, A.; Haessler, H.; Barka, A.; Ergin, M.; Türkelli, N.; Polat, O.; Üçer, S.; Kuleli, S.; Baris, S.; Kaypak, B.; Bekler, T.; Zor, E.; Bicmen, F. & Yoruk, A. (2000). The seismotectonics of the Marmara region (Turkey): results from a microseismic experiment, *Tectonophysics* **316** : 1-17.

Géli, L.; Henry, P.; Zitter, T.; Dupré, S.; Tryon, M.; Cagatay, M.; de Lépinay, B. M.; Le Pichon, X.; Sengor, A.; Gorur, N.; Natalin, B.; Ucarkus, G.; Ozeren, S.; Volker, D.; Gasperini, L.; Burnard, P.; Bourlange, S. & the Marnaut Scientific Party (2008). Gas emissions and active tectonics within the submerged section of the North Anatolian Fault zone in the Sea of Marmara, *Earth Plan. Sci. Lett.* **274** : 34-39.

Gürbüz, C., Işık, S. E., Géli, L., & Cros, E., (2013), Report On High Resolution Micro Earthquake Characterization, *Deliverable D8_2, MARSITE PROJECT, New Directions in Seismic Hazard Assessment through Focused Earth Observation in the Marmara Supersite, Grant Agreement Number: 308417, co-funded by the European Commission within the Seventh Framework Programme THEME [ENV.2012.6.4-2*], available on line: http://marsite.eu/wp-content/uploads/2012/12/D8.2.Report_On_High_Resolution_Micro_Earthquake_Characterization_submitted_lr.pdf

Hergert, T.; Heidbach, O.; Bécel, A. & Laigle, M. (2011). *Geomechanical model of the Marmara Sea regionaI. 3-D contemporary kinematics*, Geophysical Journal International 185 : 1073-1089.

Hubert-Ferrari, A.; Barka, A.; Jacques, E.; Nalbant, S. S.; Meyer, B.; Armijo, R.; Tapponnier, P. & King, G. C. P. (2000). Seismic hazard in the Marmara Sea region following the 17 August 1999 Izmit earthquake, *Nature* **404** : 269-273.

Işık,, S. E. (2014) 3D, P-wave velocity structure of the Marmara Region using local earthquake tomography, *Masters Thesis*, Bogazdici Universitesi.

Karabulut, H.; Schmittbuhl, J.; Özalaybey, S.; Lengliné, O.; Kömeç-Mutlu, A.; Durand, V.; Bouchon, M.; Daniel, G. & Bouin, M. (2011*). Evolution of the seismicity in the eastern Marmara Sea a decade before and after the 17 August 1999 Izmit earthquake*, *Tectonophysics* **510** : 17-27.

Laigle, M.; Becel, A.; de Voogd, B.; Hirn, A.; Taymaz, T. & Ozalaybey, S. (2008). *A first deep seismic survey in the Sea of Marmara: Deep basins and whole crust architecture and evolution*, Earth and Planetary Science Letters 270 : 168-179.

Le Pichon, X.; Sengor, A.; Demirbag, E.; Rangin, C.; Imren, C.; Armijo, R.; Gorur, N.; Cagatay, N.; Mercier de Lepinay, B.; Meyer, B.; Saatcilar, R. & Tok, B. (2001). *The active Main Marmara Fault*, *Earth Plan. Sci. Lett.*, **192** : 595-616.

Lomax, A., C. Satriano and M. Vassallo (2012), Automatic picker developments and optimization: FilterPicker - a robust, broadband picker for real-time seismic monitoring and earthquake early-warning, Seism. Res. Lett. , **83**, 531-540, doi: 10.1785/gssrl.83.3.531.

Lomax, A. and A. Michelini (2012), Tsunami early warning within 5 minutes, *Pure and Applied Geophysics*, **169**, doi: 10.1007/s00024-012-0512-6.

Lomax, A., A. Michelini, A. Curtis (2009), Earthquake Location, Direct, Global-Search Methods, in *Complexity In Encyclopedia of Complexity and System Science, Part 5, Springer, New York*, pp. 2449-2473, doi:10.1007/978-0-387-30440-3.

Lomax, A., J. Virieux, P. Volant and C. Berge, (2000), Probabilistic earthquake location in 3D and layered models: Introduction of a Metropolis-Gibbs method and comparison with linear locations, in *Advances in Seismic Event Location, Thurber, C.H., and N. Rabinowitz (eds.), Kluwer*, Amsterdam, 101-134

Meade, B. J.; Hager, B. H.; McClusky, S. C.; Reilinger, R. E.; Ergintav, S.; Lenk, O.; Barka, A. & Özener, H. (2002). *Estimates of Seismic Potential in the Marmara Sea Region from Block Models of Secular Deformation Constrained by Global Positioning System Measurements*, *Bull. Seism. Soc. Am.*, **92** : 208-215.

Meghraoui, M.; Aksoy, M. E.; Akyuz, H. S.; Ferry, M.; Dikbas, A. & Altunel, E. (2012). Paleoseismology of the North Anatolian Fault at Güzelköy (Ganos segment, Turkey): Size and recurrence time of earthquake ruptures west of the Sea of Marmara, *Geochemistry, Geophysics, Geosystems* **13**.

Orgülü, G. (2011). *Seismicity and source parameters for small-scale earthquakes along the splays of the North Anatolian Fault (NAF) in the Marmara Sea*, Geophysical Journal International 184 : 385-404.

Lee, W. . K., & Stewart, S. W., 1981. *Principles and applications of microearthquake networks*. Academic Press, .

Tary, J. B.; Géli, L.; Henry, P.; Natalin, B.; Gasperini, L.; Comoglu, M.; Cagatay, N. & Bardainne, T. (2011). Sea-Bottom Observations from the Western Escarpment of the Sea of Marmara, *Bull. Seism. Soc. Am.*, **101** : 775-791.

Tryon, M. D.; Henry, P. & Hilton, D. R. (2012). Quantifying submarine fluid seep activity along the North Anatolian Fault Zone in the Sea of Marmara, *Marine Geology* 315-318 : 15-28.

Waldhauser, F. & Ellsworth, W. L. (2000). A Double-Difference Earthquake Location Algorithm: Method and Application to the Northern Hayward Fault, California, *Bull. Seism. Soc. Am.*, **90** : 1353-1368.